Cellular/Molecular

DDIT4/REDD1/RTP801 Is a Novel Negative Regulator of Schwann Cell Myelination

Roberta Noseda,[1,2] **Sophie Belin,**[1] **Françoise Piguet,**[1] **Ilaria Vaccari,**[1] **Stefania Scarlino,**[1] **Paola Brambilla,**[3] **Filippo Martinelli Boneschi,**[3] **Maria Laura Feltri,**[4] **Lawrence Wrabetz,**[4] **Angelo Quattrini,**[3] **Elena Feinstein,**[5] **Richard L. Huganir,**[6] and **Alessandra Bolino**[1]

[1]Dulbecco Telethon Institute at Institute of Experimental Neurology (INSPE), San Raffaele Scientific Institute, 20132 Milan, Italy, [2]UniSR, Vita Salute San Raffaele University, 20132 Milan, Italy, [3]Institute of Experimental Neurology (INSPE), San Raffaele Scientific Institute, 20132 Milan, Italy, [4]Hunter James Kelly Research Institute, University at Buffalo, State University of New York, Buffalo, New York 14203, [5]Quark Pharmaceuticals, 70400 Ness Ziona, Israel, and [6]The Johns Hopkins University School of Medicine, Baltimore, Maryland 21205

Signals that promote myelination must be tightly modulated to adjust myelin thickness to the axonal diameter. In the peripheral nervous system, axonal neuregulin 1 type III promotes myelination by activating erbB2/B3 receptors and the PI3K/AKT/mTOR pathway in Schwann cells. Conversely, PTEN (phosphatase and tensin homolog on chromosome 10) dephosphorylates PtdIns(3,4,5)P_3 and negatively regulates the AKT pathway and myelination. Recently, the DLG1/SAP97 scaffolding protein was described to interact with PTEN to enhance PIP$_3$ dephosphorylation. Here we now report that nerves from mice with conditional inactivation of *Dlg1* in Schwann cells display only a transient increase in myelin thickness during development, suggesting that DLG1 is a transient negative regulator of myelination. Instead, we identified DDIT4/RTP801/REDD1 as a sustained negative modulator of myelination. We show that DDIT4 is expressed in Schwann cells and its maximum expression level precedes the peak of AKT activation and of DLG1 activity in peripheral nerves. Moreover, loss of DDIT4 expression both *in vitro* and *in vivo* in *Ddit4*-null mice provokes sustained hypermyelination and enhanced mTORC1 activation, thus suggesting that this molecule is a novel negative regulator of PNS myelination.

Introduction

Myelin, a highly specialized spiral membrane, ensures proper transmission of electric impulses, regulates axonal physiology, and determines the molecular domain organization of axons. Myelin-forming cells are Schwann cells in the peripheral nervous system (PNS) and oligodendrocytes in the CNS (Nave, 2010).

In the PNS, axonal neuregulin (NRG) 1 type III is one of the main signals that promotes myelination and remyelination after injury (Nave and Salzer, 2006). NRG1 type III binds to erbB2/B3 receptors in Schwann cells and transduces the signal through the PI3K/AKT (phosphatidylinositol 3-kinase/v-AKT murine thymoma viral oncogene homolog) pathway (Pereira et al., 2012). PI3K class I generates PtdIns(3,4,5)P_3 (PIP$_3$) at the plasma mem-

brane and contributes to AKT/mTOR (the mammalian target of rapamycin kinase) activation (Harrington et al., 2005; Sarbassov et al., 2005; Guertin and Sabatini, 2007; Polak and Hall, 2009). Consistent with this, overexpression of NRG1 type III causes hypermyelination with increased myelin thickness (Michailov et al., 2004). The opposite phenotype, hypomyelination with reduced myelin thickness, has been observed in *Nrg1* [+/−] and *Nrg1* [+/−]//*erbB2* [+/−] double-heterozygous mice and, more recently, in mice with Schwann cell-conditional inactivation of mTOR (Michailov et al., 2004; Taveggia et al., 2005; Sherman et al., 2012). Proper control of myelination is fundamental, as either reduced myelination (hypo/demyelination) or focal excessive myelination (hypermyelination) is associated with peripheral neuropathies (Pareyson and Marchesi, 2009).

During development, the PI3K/AKT pathway must be negatively modulated to adjust myelin thickness to axonal diameter. Indeed, PI3K/AKT activation is attenuated by the PTEN (phosphatase and tensin homolog on chromosome 10) phosphatase, which dephosphorylates PIP$_3$ in the three position, thus producing PtdIns(4,5)P_2. Accordingly, conditional inactivation of *Pten* in either Schwann cells or oligodendrocytes *in vivo* provokes sustained hypermyelination (Goebbels et al., 2010, 2012; Harrington et al., 2010). More recently, the DLG1 scaffolding protein was suggested as the main brake of PNS myelination (Cotter et al., 2010; Macklin, 2010; Roberts and Lloyd, 2012). DLG1 is believed to potentiate PTEN activity toward PIP$_3$, thus negatively modulating the AKT-mTOR pathway. Indeed, acute postnatal downregulation of *Dlg1* expression in the nerve by means of lentiviral

vector (LV) transduction leads to hypermyelination and ultimately to myelin instability (Cotter et al., 2010).

Here we report that nerves from mice with conditional inactivation of *Dlg1* in Schwann cells display only a transient increase in myelin thickness during development. Further, we identified DDIT4/RTP801/REDD1 as a novel negative modulator of myelination. In both *Drosophila* and mammalian cells, DDIT4 is known to negatively modulate the mTOR pathway by activating the tuberous sclerosis complex TSC1/2, which are GAPs for the Rheb1 GTPase (Abraham, 2005; Ellisen, 2005; Maiese et al., 2013). TSC1/2 regulation of mTORC1 activity involves phosphorylation-dependent association of TSC2 with 14-3-3 proteins and this interaction has been shown to inhibit TSC1/2 signaling to mTORC1 (mTORC1 is active). DDIT4 interacts with 14-3-3 proteins, thus inducing 14-3-3 dissociation from TSC2, activation of TSC1/2 GAPs, and inhibition of mTORC1 (DeYoung et al., 2008).

Here we report that DDIT4 upregulation in the nerve compensates for the loss of AKT/mTOR inhibition in *Dlg1*-null mice, whereas its loss both *in vitro* and *in vivo* in *Ddit4*-null mice persistently activates the mTOR pathway and causes hypermyelination.

Materials and Methods

Mice and genotyping. The generation of the *Dlg1* floxed (fl, C57/B6 strain) allele used in this study has been already reported (Zhou et al., 2008). To produce conditional knockout mice with ablation of *Dlg1* specifically in Schwann cells (*Dlg1*^fl/fl P0Cre), homozygous *Dlg1*^fl/fl mice were crossed with heterozygous *Dlg1*^fl/+ mice carrying the P0Cre transgene (Feltri et al., 1999). To obtain *Dlg1*^fl/− P0Cre conditional knockout mice (compound heterozygous for a floxed allele and a null allele), *Dlg1*^fl/+ mice were crossed with CMVCre transgenic mice and the resulting *Dlg1*^+/− mice were then crossed with *Dlg1*^fl/+ P0Cre animals.

Ddit4-null mice (C57/B6 strain) were already reported (Brafman et al., 2004). The characterization of vimentin (Vim)-null mice was also recently reported (Triolo et al., 2012). For all the experiments involving animals, $n \geq 3$ animals per genotype of either sex were analyzed. Floxed/floxed or floxed/+ or +/+ mice were independently used as controls, as littermates of knockout mice analyzed within the same experiments [indicated as "wild type" (WT) for clarity in figures].

All experiments involving animals were performed in accordance with Italian national regulations and covered by experimental protocols reviewed by local institutional animal care and use committees.

Antibodies. For Western blot analysis and immunohistochemistry, the following antibodies were used: mouse anti-DLG1 (Enzo Life Sciences), rabbit anti-PTEN (Cell Signaling Technology), rabbit anti-phospho-AKT (Ser473 and Thr308; Cell Signaling Technology), rabbit anti-AKT (pan; Cell Signaling Technology), rabbit anti-calnexin (Sigma-Aldrich), chicken anti-P0 (Millipore), mouse anti-tubulin (Sigma-Aldrich), rabbit anti-Krox20 (Covance), rabbit anti-PS6 (Cell Signaling Technology), hybridoma rat anti-MBP (kindly provided by Dr V. Lee), rabbit anti-heavy neurofilament (Millipore), rabbit anti-light neurofilament (NF-L; Covance), goat anti-REDD1 (Yoshida et al., 2010), rabbit anti-REDD1 (Epitomics), goat anti-HIF3α (Santa Cruz Biotechnology).

Secondary antibodies included peroxidase-conjugated goat anti-mouse, anti-rabbit, or anti-chicken IgG (Dako); IRDye680 and 800-conjugated goat anti-mouse and/or goat anti-rabbit IgG (Li-Cor Biosciences); fluorescein (FITC)-conjugated goat anti-rabbit IgG; and rhodamine (TRITC)-conjugated anti-rat IgG (Jackson Immunoresearch).

Protein lysates from DRG explants and purified rat Schwann cells were prepared using a lysis buffer containing the following: 1%TX-100, 50 mM Tris buffer, pH 8.0, 150 mM NaCl, 10 mM NaF, 1 mM Na vanadate, Complete (Roche) protease inhibitors. For mouse nerve lysates, a lysis buffer containing 2% SDS was used.

Schwann cell/DRG neuron cocultures. Myelin-forming Schwann cell/DRG neuron cocultures were established from embryonic day (E) 13.5 mouse embryos as previously described (Bolis et al., 2009). Briefly, DRGs were plated (1:1 ratio) on 12-mm-diameter glass coverslips (Greiner) coated with rat collagen (0.2 mg/ml; Becton Dickinson) in C media, consisting of Eagle's Minimal Essential Medium (Invitrogen) supplemented with 10% fetal calf serum (FCS; Invitrogen), 5 mg/ml glucose (Sigma-Aldrich), 50 μg/ml 2.5S nerve growth factor (NGF; Harlan or Calbiochem). DRGs were then placed in neurobasal medium (NB; Invitrogen) supplemented with B27 (Invitrogen) and NGF as before until neuritogenesis was achieved. For myelination, DRGs were placed on C media supplemented with ascorbic acid for 7–15 d (50 μg/ml; Sigma-Aldrich).

Isolated rat Schwann cells were prepared as reported previously and cultured using DMEM with 10% FCS, 2 ng/ml recombinant human neuregulin1-b1 (R&D Systems), and 2 mM forskolin (Calbiochem). To stimulate rat Schwann cells with NRG1, subconfluent cells were starved for 16 h in DMEM containing only 0.05% serum and then treated for 15 min with complete medium containing neuregulin and serum.

Immunohistochemistry. Schwann cell/DRG neuron cocultures were fixed for 15 min in 4% paraformaldehyde, permeabilized for 5 min in ice-cold methanol at −20°C, blocked for 20 min with 10% NGS, 1% BSA, and then incubated with primary antibody for 1 h. After washing, the coverslips were incubated with the secondary antibody for 30 min, washed, and mounted. For double immunostaining with anti-NF-L and anti-MBP antibody, the coverslips were blocked with 1% BSA, 10% NGS for 20 min and primary antibodies were incubated overnight at 4°C.

Analysis of myelination. To quantify the amount of myelin, ≥ 5 fields/cover were randomly acquired using a fluorescence microscope near the sensory neurons, where usually myelination is more efficient and abundant and MBP-positive myelinated fibers were counted per field. As myelination is also a function of the amount of neurites per axon and of the Schwann cell number in the culture, the network of NF-L-positive segments and the number of Schwann cells (DAPI) were also evaluated in each explant. Representative images of MBP-NF-DAPI staining have been acquired using a confocal microscope (Leica SP5).

Lentivirus preparation and infection. To downregulate *Ddit4* expression *in vitro*, nonconcentrated LVs carrying shRNA for *Ddit4* (GFP-tag) were used to transduce isolated rat Schwann cells and mouse explants (clone ID V3LMM 468446, pGIPZ vector, shRNA mir; Thermo Scientific). To produce nonconcentrated LVs, the transfer constructs were transfected into 293FT cells together with packaging plasmids Δ8.9 and pCMV-VSGV using Lipofectamine 2000 (Invitrogen). As control, a vector encoding a shRNA targeting a nonspecific sequence (luciferase) was used. Viral supernatants were collected after 72 h after transfection, centrifuged at 3,000 rpm for 15 min, and frozen at −80°C.

To check for DDIT4 depletion, freshly plated rat Schwann cells (10^6 cells per 100 mm plate) were incubated with the LVs for two consecutive overnights in DMEM, 10% FBS, and 2 mM L-glutamine plus forskolin and rhNRG-1 (EGF domain; R&D Systems). Cells were expanded for an additional week and maintained in MEM, 10% FBS, 2 mM L-glutamine, and 2 μM forskolin before use. A Western blot using an anti-REDD1 antibody was performed. Using nonconcentrated LVs, transduction of Schwann cell/DRG neuron cocultures was performed at 7 d after dissection by incubating the cells with LVs overnight. Cells were then supplemented with C media and myelination was induced after 2 d.

A concentrated LV expressing GFP-DDIT4 was used to transduce myelin-forming Schwann cell/DRG neuron cocultures [clone PLHOS-100008619 (DQ894159), concentrated LV; Thermo Scientific]. Following neuritogenesis, cells were transduced in C media using multiplicity of infection (MOI) 5–10 and myelination was then induced after 2 d.

RT-PCR analysis. Total RNA was isolated from peripheral nerve using Trizol (Life Technologies). First-strand cDNA was prepared from 1 μg of RNA using the Advantage RT-for-PCR kit (Clontech). Several independent pools containing RNA extracted from nerves of 2–5 animals were used ($n = 6$). The expression of selected mRNAs was determined by quantitative real-time PCR. Samples were processed in triplicate and reactions without target cDNA were used as negative control for each reaction. PCRs were performed on 96-well plates using the Power Sybr Green PCR Master Mix (Applied Biosystems) and following manufacturer's conditions. Designed probes were used to amplify mouse *Ddit4* and the endogenous reference transcripts calnexin. The comparative Ct method was used. As calibrator, a control sample ΔCt was chosen

for each selected transcripts. The ΔΔCt (ΔCt of each normalized selected transcript minus ΔCt of the calibrator) was calculated. Expression levels of each mRNA are indicated as $2^{-\Delta\Delta Ct}$ values. For statistical analysis, SD was calculated for triplicate samples of each reaction and SEM is indicated on the average of the determinations from different animals.

Morphological analysis. Three to five animals per genotype for each time point were analyzed. Semithin section and ultrastructural analysis of sciatic nerves was performed as reported previously (Wrabetz et al., 20005). To perform morphometric analysis, digitalized images of fiber cross sections were obtained from corresponding levels of the sciatic nerves with a Leica DFC300F digital camera with a 100× objective. Five images per animal were acquired and analyzed with the Leica QWin software (Leica Microsystem). The g ratio (axon diameter/fiber diameter) was determined by dividing the mean diameter of an axon (without myelin) by the mean diameter of the same axon including myelin.

Microarray analysis. Total RNA was extracted with Tripure Isolation Reagent (Roche).

Total RNA was quantified with NanoDrop 2000 spectrophotometer (Celbio), and its integrity was assessed by running the RNA 6000 Nano LabChip on the Bioanalyzer 2100 (Agilent Technologies) and selecting the Eukaryote Total RNA method.

The gene expression profiling was determined using the MouseWG-6 v2 Expression BeadChips (Illumina). Each beadchip can process simultaneously six samples, each one investigated for a total of 48,804 transcripts, of which 35,967 are based on the National Center for Biotechnology Information RefSeq database (Release 22) and 12,837 are based on UniGene database (Build 199). An amount of 500 ng of total RNA was reverse transcribed into cRNA and biotin-UTP labeled using the Illumina TotalPrep RNA Amplification Kit (Applied Biosystems) according to the manufacturer's protocol. Fifteen hundred nanograms of cRNA were then hybridized to the BeadChip Array and stained with streptavidin-Cy3. All procedures were performed following the manufacturer's instructions. BeadChips have been imaged using the Illumina-BeadArray Reader, a two-channel 0.8-μm-resolution confocal laser scanner, and the Illumina BeadScan software. The software Illumina-GenomeStudio v.2011.1 was used to elaborate the fluorescence signal to a value whose intensity corresponds to the quantity of the respective transcript in the original sample. The same software was used to assess the quality controls, which includes the biological specimen control, hybridization controls, signal generation controls, and negative controls. For each condition [control and *Dlg1*-null nerves at postnatal day (P) 20, P40, and 8 months], three biological replicates were tested and a scatter plot generated for each replicate set. The mean correlation coefficient of biological replicates was 0.97. Gene expression data were normalized using the quantile algorithm implemented in the IlluminaGenomeStudio v.2011.1 software, and the transcripts with an intensity value significantly different from that of background (detection *p* value, <0.01) in at least one sample were considered in the statistical analyses. A fold change of 1.5 was chosen as threshold to define the upregulated or downregulated probes in the different comparisons. The overlap of probes upregulated at P20, P40, and 8 months were represented by Venn diagrams generated using the free on-line software Venny (http://bioinfogp.cnb.csic.es/tools/venny/index.html; Pirooznia et al., 2007).

Results

Conditional inactivation of *Dlg1* in Schwann cells *in vivo* provokes transient hypermyelination

To assess whether DLG1 has a negative role on myelination *in vivo* in a more physiological context, we generated a *Dlg1*^{fl/fl} (floxed) P0Cre conditional null mouse, with *Dlg1*-specific ablation in Schwann cells starting at E13.5 (Feltri et al., 1999; Bolis et al., 2005; Zhou et al., 2008). We previously reported that Dlg1 expression in the nerve is mainly detected in Schwann cells and the Dlg1 localization pattern is regulated during development (Bolino et al., 2004; Bolis et al., 2005, 2009). We confirmed loss of Dlg1 in mutant Schwann cells at both the mRNA and protein level (Fig. 1A,B). Residual Dlg1
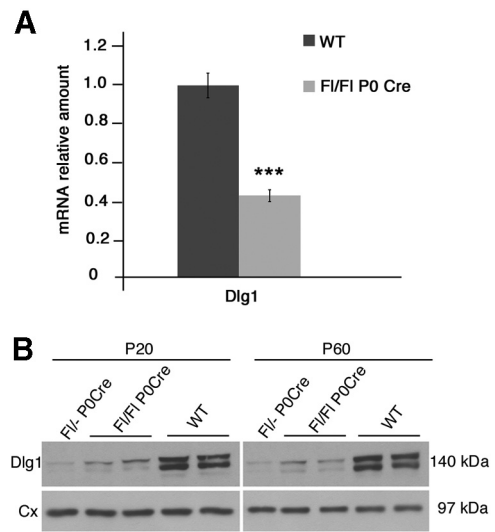

Figure 1. Loss of Dlg1 in *Dlg1*^{fl/fl} P0Cre and *Dlg1*^{fl/−} P0Cre mice. *A*, Quantitative RT-PCR analysis from *Dlg1*^{fl/fl} P0Cre nerves and controls at P20 shows a decrease of *Dlg1* mRNA ≤60% in the mutants. ****p* < 0.001. *B*, Western blot analysis on lysates from *Dlg1*^{fl/fl} P0Cre, *Dlg1*^{fl/−} P0Cre, and controls (fl/+) at both P20 and P60 demonstrates downregulation of Dlg1 at the protein level. Cx, Calnexin. All data represent means ± SEM.
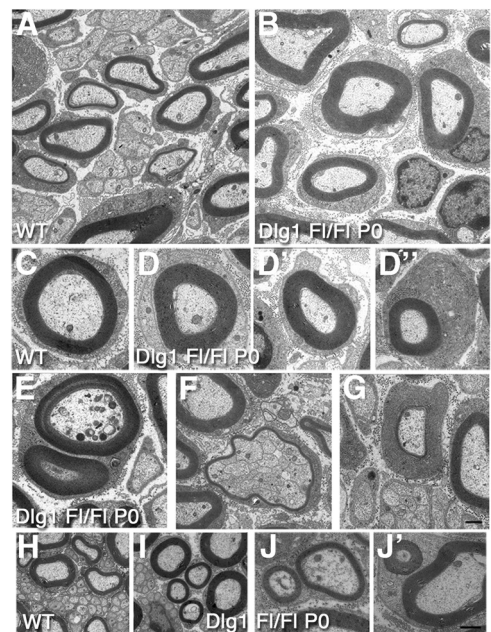

Figure 2. Ultrastructural analysis of *Dlg1*^{fl/fl} P0Cre sciatic nerves at P10. *A*, *C*, Wild-type nerve fibers. *B*, *D*, *D′*, *D″*, *Dlg1*^{fl/fl} P0Cre mutant nerves show fibers with increased myelin thickness. *E*, *F*, *G*, Myelin outfoldings (*E*), polyaxonal myelination (*F*), and uncompacted myelin (*G*) were occasionally observed in mutant nerves. *H*, *I*, Increased myelin thickness at P45 in *Dlg1*^{fl/fl} P0Cre nerves. *J*, *J′*, Occasional myelin outfoldings in *Dlg1*^{fl/fl} P0Cre nerves. Scale bars: *A–G*, 1 μm; *H–J′*, 2 μm.

expression in mutant nerve lysates might be explained by the fact that the nerve also contains perineurial cells, which express Dlg1 (Fig. 1B).

We analyzed sciatic nerves of *Dlg1*^{fl/fl} P0cre mice starting at P10. Electron microscopy analysis revealed increased myelin thickness in mutant nerve fibers (Fig. 2A–D″). Further, myelin outfoldings, polyaxonal myelination, and fibers with uncompacted myelin were occasionally observed (Fig. 2E–G). In addition to occasional myelin outfoldings, hypermyelinated fibers
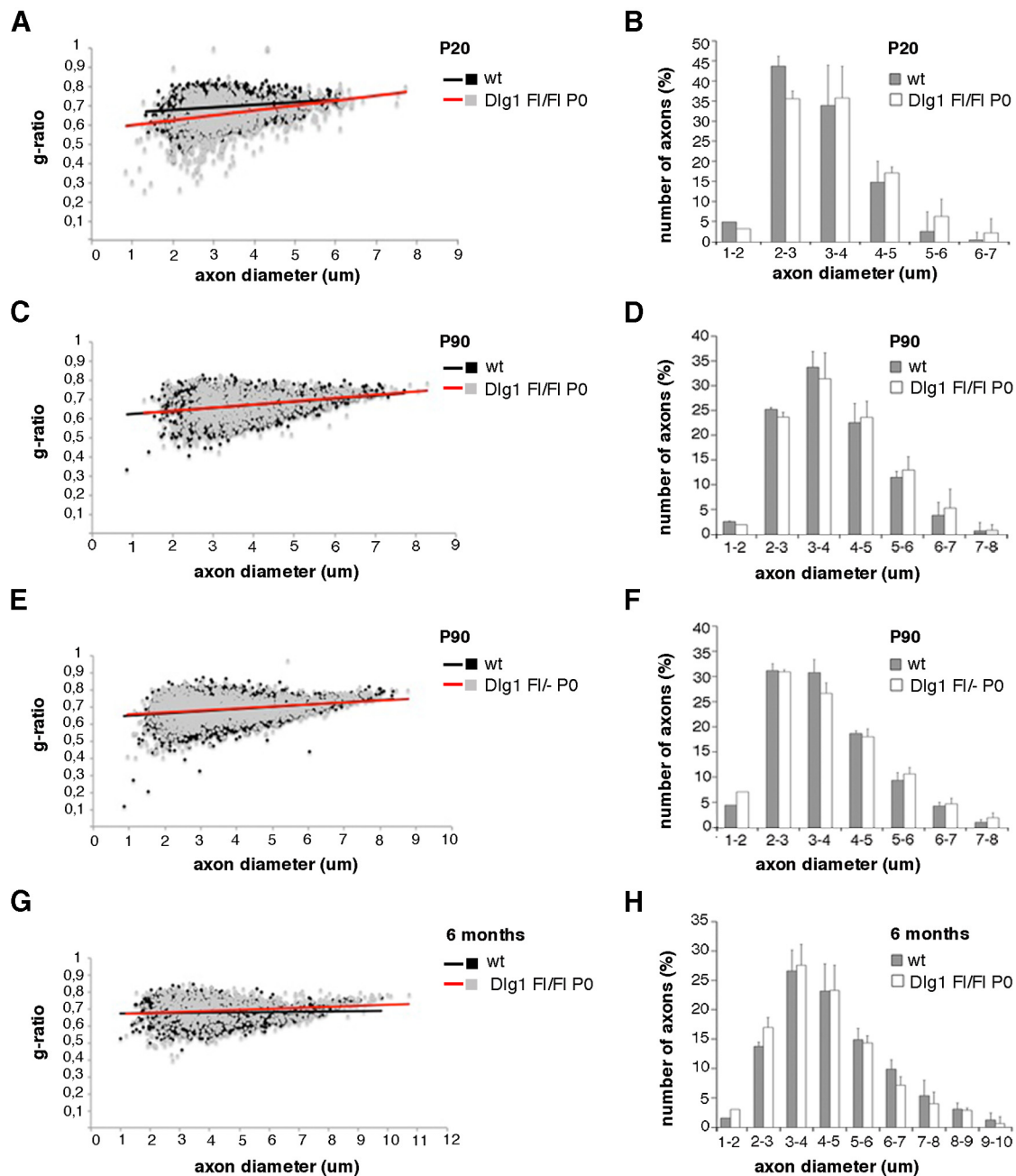
Figure 3. Transient hypermyelination in conditional *Dlg1*$^{fl/fl}$ P0Cre nerves. ***A***, Quantification of the g ratio as a function of axonal diameter in *Dlg1*$^{fl/fl}$ P0Cre sciatic nerves and controls at P20 shows increased myelin thickness in mutant nerves (*Dlg1*$^{fl/fl}$ P0Cre, 0.664 ± 0.013; WT, 0.703 ± 0.002, $p = 0.037$ on means, $n = 1500$ fibers, $n = 3$ animals per genotype). ***B***, Axonal diameter distribution at P20. ***C***, Quantification of the g ratio as a function of axonal diameter in *Dlg1*$^{fl/fl}$ P0Cre sciatic nerves and controls at P90 (*Dlg1*$^{fl/fl}$ P0Cre, 0.674 ± 0.034; WT, 0.670 ± 0.035; $p = 0.475$ on means, $n = 1600$ fibers, $n = 4$ animals per genotype). ***D***, Axonal diameter distribution at P90. ***E***, Quantification of the g ratio as a function of axonal diameter in *Dlg1*$^{fl/-}$ P0Cre sciatic nerves and control sciatic nerves at P90 (*Dlg1*$^{fl/-}$ P0Cre, 0.689 ± 0.003; WT, 0.682 ± 0.01; $p = 0.55$ on means, $n = 3000$ fibers, $n = 5$ animals per genotype). ***F***, Axonal diameter distribution at P90. ***G***, Quantification of the g ratio as a function of axonal diameter in *Dlg1*$^{fl/fl}$ P0Cre sciatic nerves and control sciatic nerves at 6 months (*Dlg1*$^{fl/fl}$ P0Cre, 0.693 ± 0.019; WT, 0.680 ± 0.019; $p = 0.61$ on means, $n = 1500$ fibers, $n = 3$ animals per genotype). ***H***, Axonal diameter distribution at 6 months. ***C, E, G***, All show normal myelin thickness in mutant nerves. All data represent means ± SEM.

were also evident at P20 and P45 (Fig. 2*H–J'*). The increase of myelin thickness in mutant nerves was further assessed by morphometric analysis (Fig. 3). The mean g-ratio value of mutant nerve fibers at P20 was significantly lower compared with wild-type nerves, thus confirming hypermyelination in *Dlg1*$^{fl/fl}$ P0Cre nerves (Fig. 3*A,B*). Increased Krox20 (at P10 and P20) and P0 myelin protein expression (at P20) in mutant nerves further supported enhanced myelination (Fig. 4*A,B*; data not shown). Finally, the number of myelinated fibers at P1–P2 was similar between mutant and wild-type sciatic nerves as assessed by both

immunohistochemistry and morphological analysis (data not shown).

DLG1 is believed to potentiate PTEN phospholipid phosphatase activity toward PIP$_3$, thus negatively modulating the PI3K/AKT signaling pathway (Cotter et al., 2010). Although PTEN expression levels were similar between mutant and control nerves at P10 (data not shown), P20, and P60 (Fig. 4*D*), AKT phosphorylation at S473 was increased in *Dlg1*$^{fl/fl}$ P0Cre nerves at P10 but not at P20, suggesting that the hypermyelinating signal is temporary (Fig. 4*C*; data not shown).
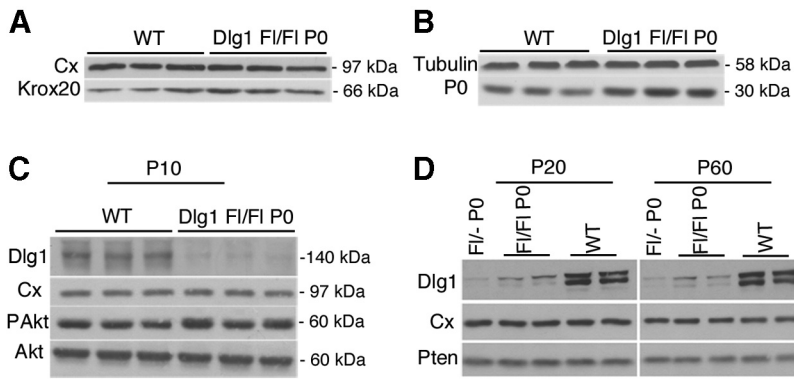
Figure 4. Enhanced myelination in *Dlg1*$^{fl/fl}$ P0Cre nerves at P10 and P20. *A*, Western blot analysis on lysates from mutant and control sciatic nerves shows increased krox20 expression in the mutant at P20 ($\leq$13%, $p = 0.043$, on 3 animals per genotype). *B*, Increased expression of P0, myelin protein zero, in mutant nerves compared with controls at P20 supports increased myelin thickness ($\leq$37%, $p = 0.0012$, on 3 animals per genotype). *C*, Increased AKT phosphorylation at S473 was observed in mutant nerves at P10 ($\leq$15%, $p = 0.05$, 3 animals per genotype). *D*, PTEN expression levels are similar between mutant and control nerves at both P20 and P60. Cx, Calnexin.
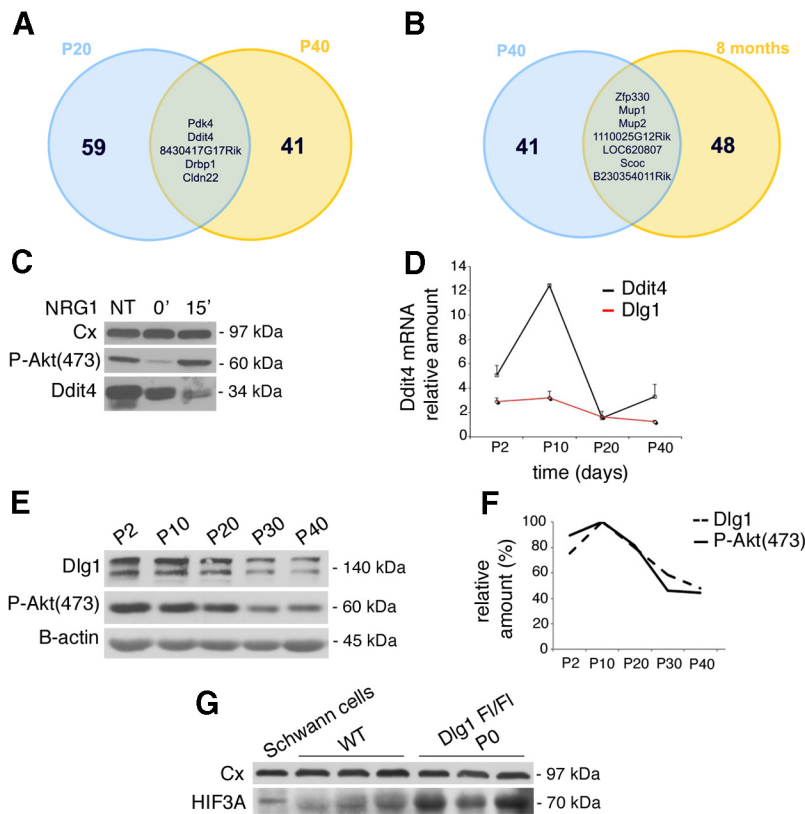

Figure 5. Upregulation of Ddit4 mRNA in *Dlg1*$^{fl/fl}$ P0Cre nerves. *A*, *B*, Venn diagrams showing upregulated number of probes for mRNA transcripts in *Dlg1*$^{fl/fl}$ P0Cre nerves compared with control nerves and shared between P20 and P40 nerves (*A*) and between P40 and 8-month-old nerves (*B*). *C*, DDIT4 is expressed in rat purified Schwann cells and its level decreases upon NRG1 stimulation for 15 min when phosphorylation of AKT at S473 increases. Cx, Calnexin. *D*, Quantitative RT-PCR analysis of *Ddit4* and *Dlg1* expression in wild-type nerves during development at P2, P10, P20, and P40, using $n = 3$ different pools per time point. *E*, *F*, Relative amount of Dlg1 and phosphorylated AKT during postnatal myelination in mouse sciatic nerves. Pools of nerves from different animals were used per time point in two independent experiments. *G*, Along with *Ddit4* upregulation, HIF3A expression also increased at both the mRNA (Table 1) and at the protein level in *Dlg1*$^{fl/fl}$ P0Cre nerves.

In fact, when analyzed at later time points, *Dlg1*-null nerves displayed normal myelination. At P90 and at 6 months of age, mean g-ratio values were similar between mutant and control nerves (Fig. 3C,D,G,H). Dlg1 expression level increases during postnatal development and myelination (Bolis et al., 2009; Cotter et al., 2010). To rule out low efficiency of Cre-mediated recom-

bination in *Dlg1*$^{fl/fl}$ P0Cre nerves, we also analyzed nerves from *Dlg1*$^{fl/-}$ P0Cre mice at P90 (Fig. 3E,F). *Dlg1*$^{fl/-}$ P0Cre conditional knockout mice are compound heterozygous for a floxed allele and a null allele (Dlg1 is lost in all cells) generated by crossing a *Dlg1*$^{fl/+}$ mouse with a CMVCre transgenic mouse. Thus, we found that also *Dlg1*$^{fl/-}$ P0Cre as *Dlg1*$^{fl/fl}$ P0Cre nerve fibers display mean G-ratio values similar to control nerves (Fig. 4E,F). In conclusion, our findings suggest that loss of *Dlg1* in Schwann cells *in vivo* leads to a transient hypermyelinating phenotype and that DLG1 acts as a temporal negative regulator of myelination in physiological conditions.

DDIT4/REDD1/RTP801 expression is upregulated in *Dlg1*$^{fl/fl}$ P0Cre nerves
We then hypothesized that the transient effect on myelination might be due to the upregulation of another negative regulator of myelination or alternatively to the downregulation of a positive regulator of myelination. To explore these possibilities, we performed a microarray analysis using mRNA from *Dlg1*$^{fl/fl}$ P0Cre sciatic nerves and controls at P20, P40, and 8 months. We selected transcripts differentially expressed of at least 1.5 folds ($p < 0.01$) in mutant nerves compared with wild type at the different time points analyzed. We also selected the mRNAs being differentially expressed in mutant nerves compared with controls and shared between P20 and P40 (when hypermyelination is still present but phosphorylation of AKT declines in *Dlg1*$^{fl/fl}$ P0Cre nerves), and between P40 and 8-month-old mutant nerves. Interestingly, the expression of other adaptors with similar function or scaffolding molecules belonging to the MAGUK (membrane-associated guanylate kinase) family, such as PSD93, PSD95, and SAP102, was normal (Sheng and Sala, 2001). Surprisingly, among the five transcripts upregulated in mutant nerves and shared between P20 and P40 mutants, we found the *Ddit4* gene (Fig. 5A,B; Table 1), which encodes REDD1/RTP801, a known negative regulator of mTORC1 and therefore an interesting candidate (Abraham, 2005; Ellisen, 2005; Maiese et al., 2013).

DDIT4-mediated regulation of mTORC1 activity has different outcomes depending on the cell type and the cellular context. In mammalian cells, *DDIT4* expression is mainly induced in response to both hypoxia and energy stress, following AMPK (AMP-activated protein kinase) activation. Further, cells defective for DDIT4 have increased mTORC1 activation and dysregulation of cell growth and cell size (Sofer et al., 2005; Yoshida et al., 2010; Cam and Houghton, 2011). More recently, it has been suggested that loss of DDIT4 in

Table 1. Genes differentially expressed in *Dlg1* fl/fl P0Cre nerves compared with controls at P20, P40, and 8 months

Illumina probe ID	Gene symbol	Mean ± SEM in WT	Mean ± SEM in KO	Fold change
P20 upregulated probes				
ILMN_2718266	Fkbp5	355 ± 25.5	1304.6 ± 481.1	2.86
ILMN_2649671	Ipas	454.1 ± 57.5	1535.1 ± 551.7	2.74
ILMN_2588249	S3-12	907.4 ± 61.2	2443.6 ± 642.9	2.47
ILMN_2969172	Tmem87a	142 ± 6.1	432.4 ± 145.3	2.42
ILMN_2822000	8430417G17Rik	260.6 ± 23.6	736.5 ± 268.3	2.26
ILMN_1229216	Zbtb16	221.5 ± 13	577.5 ± 197.7	2.19
ILMN_2701664	Dsip1	1169.3 ± 203.9	2978.2 ± 1126.5	2.04
ILMN_1246876	Kit	422 ± 90.3	964.3 ± 321.8	2.04
ILMN_1245464	Slc9a3	812.2 ± 81.4	1816.3 ± 533.8	2.03
ILMN_2466121	Twistnb	197.2 ± 71.3	359.1 ± 36.6	1.93
ILMN_1241260	D330011G23Rik	109.6 ± 2.6	249.4 ± 75.9	1.89
ILMN_1234929	Arid5b	798 ± 103.2	1633.8 ± 465.2	1.88
ILMN_2636624	8430417G17Rik	139.1 ± 6.9	307.2 ± 103.4	1.84
ILMN_1219154	Mt2	528.1 ± 62.2	1103.5 ± 359.5	1.83
ILMN_2733542	Fbxl3a	235.4 ± 10.3	556.9 ± 280	1.83
ILMN_2987862	Per2	1032 ± 183.8	1994.5 ± 575.5	1.76
ILMN_2772077	Bok	1945.6 ± 184.6	3689.2 ± 1074.5	1.76
ILMN_1231779	Twistnb	176.9 ± 58.8	293.3 ± 12	1.74
ILMN_3150811	Tsc22d3	9571.7 ± 1481.2	18,899 ± 6120.9	1.73
ILMN_2734142	Snta1	3141.2 ± 167.9	5759.4 ± 1349.8	1.72
ILMN_2636666	Prodh	871.5 ± 70.1	1579.5 ± 333.4	1.71
ILMN_2514305	Za20d1	496.5 ± 41.7	876.2 ± 136.1	1.71
ILMN_2909150	Ctgf	1696.6 ± 243.1	3093.6 ± 886.1	1.69
ILMN_1229667	Slc43a1	411.3 ± 27.8	726.3 ± 132	1.69
ILMN_2672698	Rassf4	1017.8 ± 99.2	1761.1 ± 318.7	1.68
ILMN_1238215	Ctgf	1141.8 ± 175.6	2043.9 ± 585.5	1.67
ILMN_1240671	LOC382058	262.9 ± 40.6	515.2 ± 200.1	1.67
ILMN_3122383	Otud7b	1594.9 ± 119.1	2811.8 ± 607.7	1.67
ILMN_2689160	Ranbp9	983.4 ± 26	1738.2 ± 378.7	1.67
ILMN_1259322	Pdk4	619.6 ± 225.9	1014.8 ± 282.4	1.67
ILMN_2770894	Map3k6	343 ± 12.1	600.2 ± 106.9	1.66
ILMN_3046773	Otud7b	364.8 ± 21	639.7 ± 122.7	1.66
ILMN_1243942	LOC382190	231.8 ± 118.9	371.4 ± 131.3	1.63
ILMN_2430906	2310051E17Rik	734.7 ± 31.8	1257.5 ± 276.8	1.62
ILMN_2760494	Hif3a	137.4 ± 9	247.1 ± 59.8	1.61
ILMN_2693835	Arrdc2	420.1 ± 52.7	735 ± 188.4	1.61
ILMN_2947292	Map3k6	328.7 ± 13.8	563.8 ± 113.3	1.61
ILMN_2987863	Per2	791.2 ± 147.7	1366.6 ± 369.2	1.61
ILMN_1237404	Bok	219.6 ± 24.1	372.4 ± 73.8	1.60
ILMN_2768972	BC055107	3198 ± 387.7	5351.7 ± 1182.9	1.60
ILMN_3163340	Drbp1	299.1 ± 2.6	516.1 ± 114.6	1.59
ILMN_2964560	Cd163	741.2 ± 33.9	1195.6 ± 138.7	1.58
ILMN_1218051	A630086H07Rik	2709.3 ± 223.8	4340.4 ± 567.4	1.58
ILMN_2838308	Fmo1	2734.5 ± 359	4384.6 ± 747.8	1.58
ILMN_1253819	Prkar2b	2329.6 ± 390.9	3572.9 ± 200.9	1.57
ILMN_2944508	Bglap2	263.4 ± 105.6	576.8 ± 384.5	1.57
ILMN_3136744	Sesn1	6700 ± 226.8	10,904.7 ± 1976.8	1.57
ILMN_1225370	2410039M03Rik	4132.3 ± 249.6	7034.8 ± 1790.3	1.57
ILMN_1254031	Bteb1	7259.8 ± 462.6	11,955.6 ± 2839.1	1.56
ILMN_2723891	Egfl5	1677.1 ± 107	2630.7 ± 339.8	1.55
ILMN_2894211	8430408G22Rik	381.1 ± 110.7	610.4 ± 166	1.54
ILMN_2993109	Ddit4	3411 ± 713.9	6097.5 ± 2258.9	1.53
ILMN_2688681	Npm3	310.9 ± 50.9	502.3 ± 119.6	1.52
ILMN_2636738	Fstl3	468.3 ± 29.6	739.6 ± 128.2	1.51
ILMN_2476733	1200016E24Rik	2417.1 ± 182.9	3825.8 ± 793.8	1.51
ILMN_2753912	Pdgfc	231.3 ± 12.5	367.9 ± 62.7	1.51
ILMN_2908846	Iqgap2	1290.4 ± 89.1	1959.7 ± 195.4	1.50
ILMN_1221999	Cldn22	972.2 ± 172	1451.5 ± 182.8	1.50
ILMN_1217629	Itgae	371.7 ± 11.5	585 ± 101.8	1.50
P40 upregulated probes				
ILMN_2838965	4930455C21Rik	484.3 ± 249.4	689.4 ± 201.2	3.37
ILMN_2965669	Xlr4a	443.5 ± 168.4	584.1 ± 69.3	2.77

(*Table continues.*)

Table 1. Continued

Illumina probe ID	Gene symbol	Mean ± SEM in WT	Mean ± SEM in KO	Fold change
ILMN_2825109	Zfp330	720.6 ± 291	828.9 ± 283.5	2.63
ILMN_2543433	1110030C22Rik	831.5 ± 211.1	1035.3 ± 383.3	2.32
ILMN_2672772	Abhd1	225 ± 63.3	255.8 ± 67.8	2.04
ILMN_2676379	Pon1	459.8 ± 109	553.5 ± 425	1.93
ILMN_2729513	Hbb-b2	121.5 ± 5	149.2 ± 98.3	1.89
ILMN_2672778	Abhd1	222.1 ± 62.1	235.8 ± 51.2	1.86
ILMN_3065459	Mup2	1662.1 ± 283.3	2009.8 ± 1358.7	1.83
ILMN_2953807	LOC620807	1011.4 ± 135.7	1243.1 ± 886.1	1.81
ILMN_1246772	B430305P08Rik	1232.5 ± 230	1282.7 ± 200.4	1.81
ILMN_1245678	Abhd1	291.7 ± 72.5	303.8 ± 75.1	1.79
ILMN_1234241	1110025G12Rik	302.9 ± 75.4	311.1 ± 44.1	1.78
ILMN_2875730	Mup1	3058 ± 520.6	3767.4 ± 2804	1.77
ILMN_1229990	Agxt2l1	211.4 ± 55.5	217.4 ± 39	1.76
ILMN_3111685	Acsm3	217 ± 38	241.4 ± 135.8	1.74
ILMN_3143404	Mup2	936.4 ± 141.5	1135.2 ± 831.8	1.74
ILMN_2893879	Gdpd3	880.3 ± 278.4	929.1 ± 470.4	1.74
ILMN_1223046	Cdgap	184.5 ± 38.7	190.7 ± 37.5	1.73
ILMN_2648669	Gpnmb	1522.5 ± 97.2	1568.9 ± 348.3	1.71
ILMN_2627318	4930455C21Rik	245.9 ± 50.6	249.1 ± 35	1.70
ILMN_2730208	Mup1	9221.5 ± 1425.1	10,992.6 ± 8277.7	1.70
ILMN_1225291	B230354O11Rik	1162.1 ± 615.7	1010 ± 51.5	1.69
ILMN_2540464	LOC381904	191 ± 11	236.2 ± 247.8	1.66
ILMN_1229454	Cuedc1	398.8 ± 68.7	395 ± 100.9	1.63
ILMN_1216231	Scoc	521.4 ± 95.8	514.7 ± 132.6	1.63
ILMN_3135697	1200003I07Rik	736.3 ± 167	704 ± 76.2	1.63
ILMN_1225130	LOC385909	123.5 ± 9.9	125.3 ± 17.6	1.62
ILMN_2702903	Cyp2f2	521.2 ± 100.3	512 ± 145.4	1.62
ILMN_2944824	Hp	2262.5 ± 449.5	2240.5 ± 892.2	1.61
ILMN_1259322	Pdk4	564.4 ± 95.3	546.1 ± 123.2	1.58
ILMN_2993109	Ddit4	1800.5 ± 103.5	1833.8 ± 905.5	1.57
ILMN_1251114	BC002216	208.9 ± 111.5	192.6 ± 111.4	1.54
ILMN_2668509	Hp	1267 ± 184.2	1239.4 ± 519.8	1.54
ILMN_1241214	Myh4	168.6 ± 38.2	205.9 ± 235	1.54
ILMN_2822000	8430417G17Rik	492.1 ± 63.7	469.4 ± 96.5	1.52
ILMN_2772273	Cldn22	769 ± 202.8	701.6 ± 142	1.52
ILMN_2676012	Mybpc2	309.1 ± 124	391.4 ± 517.9	1.52
ILMN_2458376	5330426P16Rik	159 ± 14.1	155.1 ± 39.6	1.52
ILMN_3163340	Drbp1	361.6 ± 103.8	358.9 ± 203.2	1.51
ILMN_1221146	4930443F05Rik	275.5 ± 73.7	254.3 ± 38.4	1.51
8 month upregulated probes				
ILMN_1215076	F830002E14Rik	7663.5 ± 2723.4	24,735.2 ± 5724	3.50
ILMN_2825109	Zfp330	439.7 ± 293.1	978.7 ± 29.4	3.29
ILMN_1235372	Hbb-b1	1377.8 ± 724.2	4437.8 ± 2371.4	2.99
ILMN_2544056	Hbb-b1	4736.6 ± 2157.2	18,237.3 ± 11,394.8	2.71
ILMN_2675874	Alas2	676.8 ± 205.9	2201.9 ± 1242.8	2.35
ILMN_2875730	Mup1	680.5 ± 443	2320.3 ± 1725.9	2.24
ILMN_1241039	2510042H12Rik	191.8 ± 47.6	593.6 ± 338.5	2.22
ILMN_1228607	Igk-V1	234.1 ± 44.8	1263.1 ± 1058.6	2.19
ILMN_2730208	Mup1	2126.8 ± 1515.1	7288.1 ± 5425.7	2.17
ILMN_1255462	Hbb-b1	29,863.5 ± 15,173.6	52,608.5 ± 10,818.9	2.16
ILMN_1250715	LOC381774	198.2 ± 45.3	1086.1 ± 918.2	2.14
ILMN_2539917	LOC384538	202.2 ± 42.5	578.9 ± 302.6	2.10
ILMN_3065459	Mup2	366.9 ± 198.4	1114.9 ± 745.9	2.10
ILMN_2631259	Igk-V1	166.1 ± 10.8	455.4 ± 251	1.97
ILMN_2769490	5430435G22Rik	445.6 ± 107.8	822.6 ± 207.2	1.84
ILMN_1234241	1110025G12Rik	576.5 ± 191.6	1029.1 ± 364.1	1.81
ILMN_2953807	LOC620807	303.4 ± 141.1	691.9 ± 392.2	1.80
ILMN_1216231	Scoc	350.1 ± 97	595.6 ± 14.3	1.78
ILMN_1256775	Thrsp	1232.6 ± 277	2694.8 ± 1130.4	1.76
ILMN_2484987	Man2b1	1189.2 ± 450.4	1645.7 ± 43.7	1.76
ILMN_1239117	Hbb-b1	31,967.3 ± 12,718.4	50,064.2 ± 9739.4	1.76
ILMN_2502614	Ttc15	144.8 ± 31.6	261.1 ± 34.2	1.76
ILMN_1216452	Hbb-b1	31,229.4 ± 12,824.9	49,044.9 ± 12,004.8	1.74

(*Table continues.*)

Table 1. Continued

Illumina probe ID	Gene symbol	Mean ± SEM in WT	Mean ± SEM in KO	Fold change
ILMN_2777462	Adpn	525.7 ± 116.7	1041.7 ± 452.2	1.71
ILMN_1226935	Orm1	835.4 ± 125.6	1459.3 ± 264.6	1.71
ILMN_3143404	Mup2	286.6 ± 138	696.5 ± 464.7	1.70
ILMN_1226583	LOC384422	94.8 ± 0.8	205.9 ± 97.4	1.68
ILMN_2545963	Hbb-b1	37,692.8 ± 14,022.3	56,316.9 ± 8010.8	1.68
ILMN_1215901	Agpat2	1235.1 ± 176.8	2058.4 ± 255.1	1.66
ILMN_1255372	LOC386321	136.1 ± 1.7	251.2 ± 56.2	1.66
ILMN_1225291	B230354011Rik	1667.1 ± 576.7	2453.2 ± 606	1.63
ILMN_1230696	Igl-V1	115.6 ± 1.4	317.8 ± 221.5	1.62
ILMN_1245146	Igl-V1	217.8 ± 35.1	954.5 ± 830.8	1.62
ILMN_1228020	1500010G04Rik	428.2 ± 87	672.4 ± 31.5	1.60
ILMN_1212702	Hba-a1	34,308.3 ± 10,714.2	51,271.2 ± 9519.5	1.58
ILMN_2616584	Ppp1r1a	595.2 ± 173.9	958.3 ± 272.7	1.57
ILMN_1223244	Hbb-b1	37,626.7 ± 12,767.1	53,585 ± 9091.1	1.55
ILMN_1224207	D630016K15Rik	195.9 ± 44.9	330.8 ± 101.7	1.55
ILMN_1247691	Hes1	711.8 ± 37	1112.6 ± 62	1.55
ILMN_1229203	Hbb-b1	40,393.6 ± 12960.1	56,895.9 ± 8213.5	1.53
ILMN_2740151	Chpt1	1799.6 ± 168.8	2769.5 ± 274.8	1.53
ILMN_2777535	Ptplb	742.2 ± 45.5	1178.1 ± 219.8	1.53
ILMN_2692644	BC054059	839.2 ± 197.8	1400.1 ± 438.8	1.53
ILMN_2599794	Apoc1	723.1 ± 172.6	1326.7 ± 646.7	1.52
ILMN_2886260	Foxc1	773.4 ± 104	1172 ± 124.1	1.52
ILMN_1219915	Dgat2	6132.1 ± 630.8	9250.4 ± 828.8	1.51
ILMN_1236603	LOC386169	228.6 ± 22.5	350.9 ± 21.6	1.51
ILMN_1226472	Retnla	2319.5 ± 311.7	3593 ± 748.1	1.50

neurons affects survival and the timing of neuronal differentiation and migration (Shoshani et al., 2002; Brafman et al., 2004; Malagelada et al., 2011).

To assess the role of DDIT4 in the PNS, we first determined its expression *in vitro* and *in vivo*. We found that DDIT4 is expressed in rat purified Schwann cells (Fig. 5C), whereas *in vivo* in the nerve, *Ddit4* mRNA expression is significantly upregulated between P2 and P10 and then rapidly declines between P10 and P20 (Fig. 5D). Interestingly, NRG1 stimulation of rat purified Schwann cells reduces DDIT4 expression along with an increase of AKT phosphorylation at S473 (Fig. 5C). This finding indicates that DDIT4 expression likely precedes the peak of AKT activation both *in vitro* and *in vivo* (Fig. 5D–F). Unfortunately, DDIT4 protein expression was not further investigated *in vivo*, as available antibodies were not specific when used on nerve.

The upregulation of the *Ddit4* gene in *Dlg1*$^{fl/fl}$ P0Cre nerves was further confirmed by quantitative RT-PCR analysis (controls, 1 ± 0.084; *Dlg1*$^{fl/fl}$ P0Cre, 1.424 ± 0.091; $p = 0.005$, on seven pools of three animals per genotype). To assess whether the upregulation of *Ddit4* expression was a consequence of the loss of Dlg1 or rather a general phenomenon associated with hypermyelination mediated by the PI3K/AKT/mTOR pathway, we analyzed *Ddit4* mRNA expression in *Vim*-null nerves, characterized by increased NRG1 type III signaling leading to sustained hypermyelination (Triolo et al., 2012). In *Vim*-null nerves, *Ddit4* expression was similar to that of control (controls, 1.22 ± 0.17; *Vim* null, 1.07 ± 0.091; $p = 0.578$, on seven pools of three animals per genotype), suggesting that the upregulation of *Ddit4* observed in *Dlg1*$^{fl/fl}$ P0Cre nerves is due to the loss of Dlg1 rather than to a general event linked to hypermyelination.

Interestingly, along with increased expression of *Ddit4*, we also found that HIF3α (hypoxia inducible factor) is significantly upregulated in *Dlg1*$^{fl/fl}$ P0Cre nerves at P20 at both the mRNA (Table 1) and protein level (Fig. 5G). In addition to hypoxia, also mTORC1 can induce HIF1α and DDIT4 expression, thus eliciting a negative feedback loop on its own activity (Ellisen, 2005; Schwarzer et al., 2005). Although the role of HIF3α still remains to be assessed (Hatanaka et al., 2009; Tanaka et al., 2009), it can be hypothesized that following AKT/mTOR activation, HIF3α induces DDIT4 expression in *Dlg1*$^{fl/fl}$ P0Cre nerves, which negatively regulates the mTOR pathway, leading to normal myelin thickness at later stages.

DDIT4 is a negative regulator of myelination *in vitro*

Because of its role as a negative regulator of mTORC1 in other systems, DDIT4 could potentially negatively regulate myelination in the PNS. To investigate DDIT4 function in myelination, we first established myelin-forming Schwann cell/DRG neurons cocultures from *Dlg1*$^{fl/fl}$ P0Cre and control mouse embryos at E13.5. To increase P0Cre-mediated recombination *in*
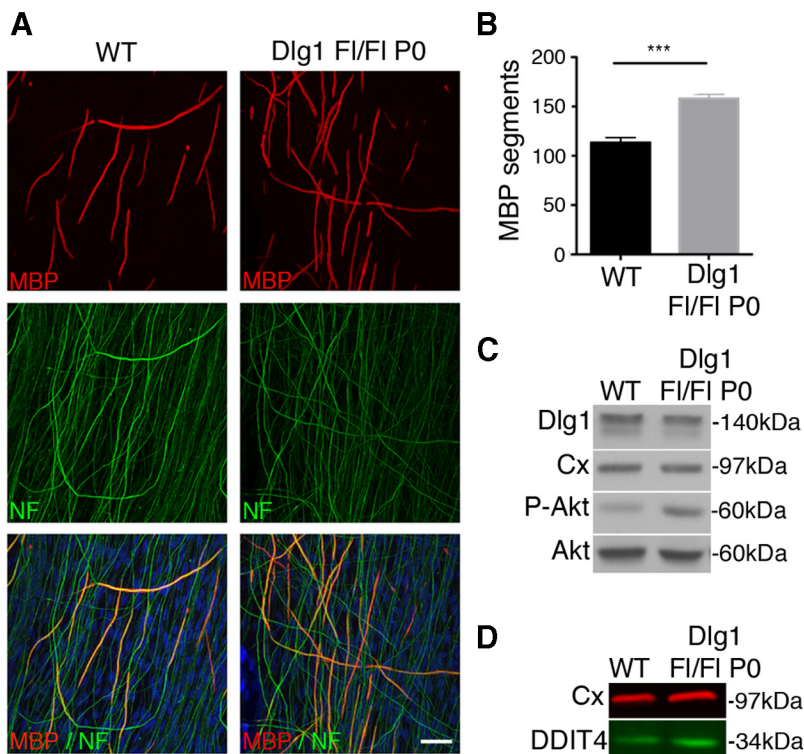

Figure 6. Increased myelination in *Dlg1*$^{fl/fl}$ P0Cre Schwann cell/DRG neuron cocultures. **A**, Cocultures established from *Dlg1*$^{fl/fl}$ P0Cre embryos produced more myelinated segments compared with control cultures. Cells were cultured for 10–15 d in NB and myelination was induced for 7 or 15 d with ascorbic acid. **B**, In all conditions, an increase of ~40% of MBP-positive fibers was scored in mutant cultures, $n = \geq 10$ covers/DRG per genotype, four different experiments. ***$p < 0.001$, data represent means ± SEM. **C**, Western blot analysis on lysates from mutant and wild-type cocultures shows decreased Dlg1 expression and increased phosphorylation of AKT (S473) in mutant cells, which is consistent with *in vivo* findings. **D**, DDIT4 expression is upregulated in *Dlg1*$^{fl/fl}$ P0Cre cultures (WT, 0.616; *Dlg1*$^{fl/fl}$ P0Cre, 0.8963, ≤45%). Lysates from pools of at least 10 different covers/DRG per genotype were loaded. Cx, Calnexin. Scale bar, 10 μm.
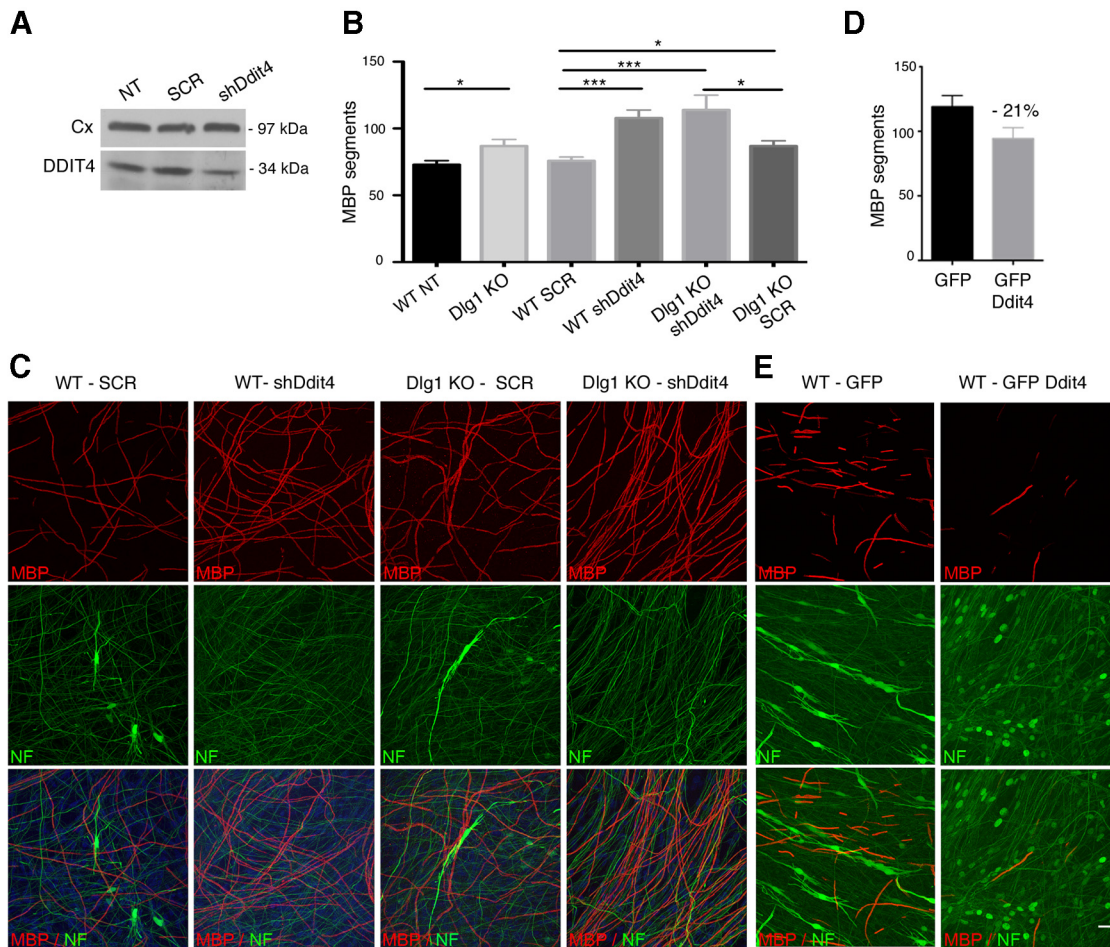
Figure 7. DDIT4 is a negative regulator of myelination *in vitro* in myelin-forming Schwann cell/DRG neuron cocultures. *A*, Efficiency of DDIT4 downregulation using *Ddit4* shRNA LV on purified rat Schwann cells. Cx, Calnexin. *B*, *C*, Wild-type cultures transduced with LV carrying GFP-*Ddit4* shRNA produced more myelinated segments compared with scramble (GFP-tag)-treated cultures. Similarly, cocultures established from *Dlg1*^{fl/fl} P0Cre mouse embryos transduced with *Ddit4* shRNA LV yielded more myelinated segments compared with *Dlg1*^{fl/fl} P0Cre cultures transduced with a scramble sequence. Note that *Dlg1*^{fl/fl} P0Cre explants in *B* produced 19% more MBP segments than control explants and not 40% as reported in Figure 7. In this experiment explants were transduced after 7 d of NB treatment. WT NT (not transduced) and Dlg1 KO, $p = 0.027$; WT SCR (scramble) and WT shDdit4, $p < 0.0001$; WT SCR and Dlg1 KO shDdit4, $p = 0.0006$; Dlg1 KO shDdit4 and Dlg1 KO SCR, $p = 0.0356$; WT SCR and Dlg1 KO SCR, $p = 0.0274$. *D*, *E*, The overexpression of GFP-DDIT4 by means of LV transduction in wild-type cultures significantly decreased the number of myelinated segments. MBP is myelin basic protein. The mean of MBP-positive segments scored in the cultures is reported $\pm$ SEM. Experiments have been scored using $\leq n = 10$ different DRGs per condition. Scale bars, 10 μm.

vitro, *Dlg1*^{fl/fl} P0Cre explants were cultured for 15 d in NB medium before inducing differentiation by ascorbic acid treatment. *Dlg1*^{fl/fl} P0Cre explants produced significantly more myelinated segments after 7 and 15 d of ascorbic acid treatment compared with control, thus reproducing the hypermyelination observed *in vivo* (Fig. 6*A*,*B*). Consistent with this finding, AKT phosphorylation at S473 was increased in *Dlg1*^{fl/fl} P0Cre explants (Fig. 6*C*). Interestingly, DDIT4 expression was upregulated in *Dlg1*^{fl/fl} P0Cre explants (Fig. 6*D*).

To assess the role of DDIT4, we downregulated *Ddit4* expression by means of shRNA LV transduction in either wild-type or *Dlg1*-null explants. In this case, *Dlg1*^{fl/fl} P0Cre and wild-type explants were infected after 7 d in culture and ascorbic acid was provided at day 10 for 7 d. Ablation of *Ddit4* in wild-type explants produced significantly more myelinated segments compared with scramble-treated controls (Fig. 7*A–C*). Interestingly, downregulation of *Ddit4* expression in *Dlg1*^{fl/fl} P0Cre explants resulted in more myelin segments compared with both *Dlg1*^{fl/fl} P0Cre explants transduced with a scramble sequence and to wild-type explants (Fig. 7*A–C*). Finally, we overexpressed GFP-DDIT4 in premyelinating cocultures in which neuritogenesis was already

achieved. Cultures transduced with GFP-DDIT4 LVs yielded significantly fewer myelinated segments compared with GFP transduced cultures (Fig. 7*D*,*E*). Overall, these findings suggest that DDIT4 is a negative regulator of myelination *in vitro*.

Loss of *Ddit4 in vivo* causes sustained hypermyelination in the PNS

To assess the role of DDIT4 *in vivo*, we analyzed sciatic nerves of *Ddit4*-null mice starting at P10 (Shoshani et al., 2002; Yoshida et al., 2010). In *Ddit4*-null nerves at P10, we observed fibers with increased myelin thickness, whereas the number of myelinated fibers was similar between mutant and control nerves (Fig. 8*A*). Additional signs of enhanced or ectopic myelination, such as polyaxonal myelination and myelinated fibers <1 μm were not evident. G-ratio analysis performed at P30 and at P90 confirmed increased myelin thickness in *Ddit4*-null nerves, whereas the total number of myelinated fibers and fiber diameter distribution were similar between mutant and control nerves (Fig. 8*C–H*). Interestingly, signs of focal hypermyelination, such as tomacula or myelin outfoldings, which are linked to PI3K/AKT/mTOR acti-
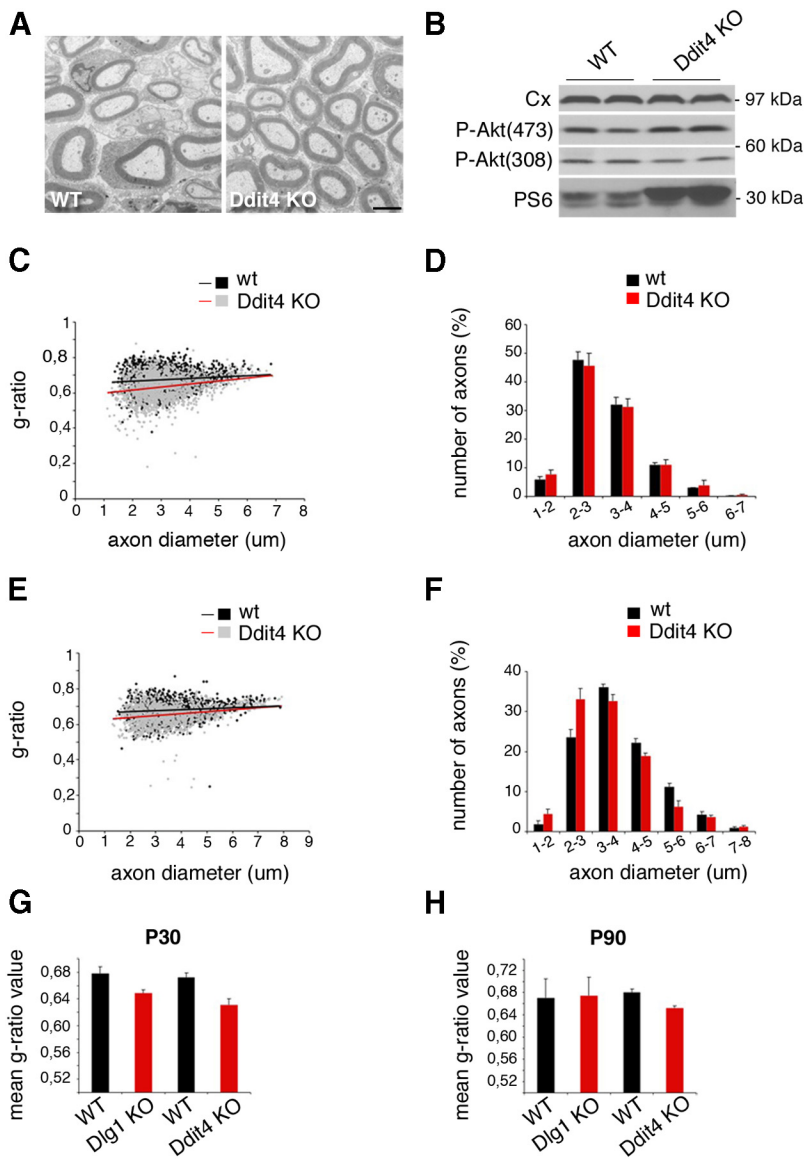
Figure 8. Loss of *Ddit4 in vivo* leads to sustained hypermyelination with increased myelin thickness in the nerve. *A*, Ultrastructural analysis of *Ddit4*-null sciatic nerves at P10 shows fibers with increased myelin thickness. *B*, Western blot analysis showing increased S6 in *Ddit4*-null nerves (≤50%; WT, 0.48 ± 0.043; *Ddit4*-null, 0.98 ± 0.069) and AKT (S473), and decreased AKT (T308) phosphorylation in *Ddit4*-null nerves (S473 phosphorylation: ≤30%; WT, 0.725 ± 0.021; *Ddit4*-null, 0.94 ± 0.001; T308 phosphorylation: ≤10%, WT, 0.64 ± 0.092; *Ddit4*-null, 0.50 ± 0.046) compared with controls, suggesting mTORC1 activation. Cx, Calnexin. *C*, Quantification of the g ratio as a function of axonal diameter in *Ddit4*-null sciatic nerves and control sciatic nerves at P30 (*Ddit4*-null, 0.631 ± 0.009; WT, 0.672 ± 0.007, $p = 0.026$ on means, $n = 2000$ fibers, $n = 4$ animals per genotype) shows increased myelin thickness in mutant nerves. *D*, Axonal diameter distribution at P30. *E*, Quantification of the g ratio as a function of axonal diameter in *Ddit4*-null sciatic nerves and control sciatic nerves at P90 (*Ddit4*-null, 0.652 ± 0.004; WT, 0.680 ± 0.007, $p = 0.02$ on means, $n = 1500$ fibers, $n = 3$ animals per genotype) shows increased myelin thickness in mutant nerves. *F*, Axonal diameter distribution at P90. *G*, *H*, Comparison between mean g-ratio values of *Dlg1*$^{fl/fl}$ P0Cre and *Ddit4*-null nerves at P30 (*G*) and at P90 (*H*) indicates that hypermyelination is transient in *Dlg1*$^{fl/fl}$ P0Cre whereas represents a sustained phenotype in *Ddit4*-null nerves. At P30, mean g-ratio value is 0.649 ± 0.005 for *Dlg1*$^{fl/fl}$ P0Cre nerves and 0.678 ± 0.01 for control nerves ($n = 1700$ fibers, 3 animals). Scale bar, 2 μm. All data represent means ± SEM.

vation, were not observed in *Ddit4*-null nerves at any time points analyzed.

DDIT4 activates TSC1/2 GAPs and negatively regulates mTORC1 (Abraham, 2005; Ellisen, 2005; Maiese et al., 2013). To investigate the extent of mTORC1 activation in *Ddit4*-null nerves, we looked at the phosphorylation of the S6 kinase, a downstream target of mTORC1. We found that phosphorylation of S6 was significantly increased in *Ddit4*-null nerves, suggesting

activation of the mTOR pathway (Fig. 8*B*). Phosphorylation of AKT at residue 473 was increased in mutant nerves, consistent with mTORC2 activation by mTORC1 and the positive feedback loop on AKT phosphorylation. Further, AKT phosphorylation at T308 was slightly decreased in the mutant, likely as the result of a negative feedback loop on tyrosine kinase receptors and PDK1 activation (Harrington et al., 2005).

In conclusion, our results support a role for DDIT4 as a negative regulator of myelination, as its loss both *in vitro* and *in vivo* results in hypermyelination.

Discussion

During development, myelination is promoted by a plethora of positive signals, which must be tightly modulated to ensure a correct timing for myelination and to adjust myelin thickness to the axonal diameter.

In the PNS, axonal NRG1 type III dictates the differentiating fate of a Schwann cell and, above a certain threshold, the amount of myelin that has to be produced. NRG1 type III binds to erbB2/B3 receptors in Schwann cells, of which the PI3K/AKT pathway is one of the main downstream effectors (Nave and Salzer, 2006; Pereira et al., 2012). DLG1 has been recently suggested as the main brake on myelination in the PNS by acting on the modulation of the PI3K/AKT pathway (Cotter et al., 2010; Macklin, 2010). DLG1 is believed to potentiate PTEN enzymatic activity toward PIP$_3$, which contributes to AKT activation (Cotter et al., 2010). Indeed, Cotter et al. (2010) reported that acute postnatal downregulation of Dlg1 expression by injecting LVs in sciatic nerves at both P3 and P20 results in increased myelin thickness at 2 months and 3 weeks postinjection, respectively. Loss of DLG1 should lead to decreased PTEN activity, increased PIP$_3$ levels, sustained AKT activation, and hypermyelination.

Consistent with the previous report, we found that nerves from mice with *Dlg1* conditional inactivation in Schwann cells are hypermyelinated, with a mild but significant increase in myelin thickness during postnatal development. However, in contrast with previous findings, adult *Dlg1*-null nerves displayed normal myelin thickness, suggesting that the hypermyelination is transient and related to the developmental stage. Further, Cotter et al. (2010) reported that DLG1 regulates PTEN stability and amount *in vitro*. However, in *Dlg1*-null nerves we observed normal PTEN expression. Our results might be explained by the fact that, when the DLG1 is lost in a more physiological context, PTEN enzymatic activity rather than its expression level may change, as already reported for other enzymes

regulating phosphatidylinositide (PI) metabolism (Zolov et al., 2012).

Interestingly, we also found that in *Dlg1*-null nerves *Ddit4* expression is upregulated. DDIT4/REDD1/RTP801 attracted our attention as DDIT4 is a known negative regulator of the mTOR pathway in other cells (Abraham, 2005; Ellisen, 2005; Maiese et al., 2013) and thus a potential negative regulator of myelination mediated by the PI3K-AKT pathway. This protein was independently identified in human as direct transcriptional target of HIF and in *Drosophila* as *Shylla* and *Charydbis*, two orthologues of *Ddit4*, encoding TSC-dependent potent suppressors of PI3K (Sofer et al., 2005; Yoshida et al., 2010; Cam and Houghton, 2011). While the regulation of mTOR by PI3K/AKT does not require DDIT4 under nutrients and growth factor stimulation, following hypoxia and energy stress mTOR activity is dependent on DDIT4. In addition, DDIT4 is involved in the control of cell size and cell growth, as overexpression or RNAi-mediated inhibition of DDIT4 in both *Drosophila* and mammalian cells impair cell size and growth. Interestingly, in neurons DDIT4 role varies depending on the cellular context. DDIT4 protects neurons from apoptosis following oxidative stress, may promote death of postmitotic neurons, and regulates the timing of cortical neurogenesis and neuron migration (Malagelada et al., 2011).

Given its role as negative regulator of the AKT/mTOR pathway in other cells, DDIT4 represented a novel candidate to negatively regulate PNS myelination. Indeed we found that the downregulation of *Ddit4* expression in myelin-forming Schwann cell/DRG neuron cocultures enhances myelination. Further, overexpression of DDIT4 in a coculture system led to decreased myelination. In addition, we confirmed that DDIT4 is a negative regulator of myelination *in vivo*, as *Ddit4*-null nerves displayed enhanced mTORC1 activation and increased myelin thickness during development as well as in adult nerves.

DDIT4 and DLG1, two negative regulators of myelination
The fact that DLG1 and DDIT4 act on the same pathway and that *Ddit4* is upregulated in *Dlg1*^{fl/fl} P0Cre nerves suggests that DLG1 and DDIT4 are functionally linked.

In cultured neurons, DDIT4 levels increase soon after NGF stimulation, but rapidly decline when neuronal differentiation takes place (Malagelada et al., 2011). Moreover, it has been recently reported that *in vitro* and *in vivo* interference with DDIT4 expression promotes cell cycle exit and accelerates neuronal differentiation (Malagelada et al., 2011). To assess whether DDIT4 may also control the timing of differentiation and myelination at early stages in Schwann cells, we measured *Ddit4* expression pattern during postnatal nerve development. We found that *Ddit4* expression reaches its maximum level between P2 and P10, and then rapidly drops between P10 and P20. Thus the *Ddit4* expression level anticipates the peak of AKT phosphorylation and activation and of DLG1 expression/stability. Therefore, it can be speculated that, by analogy with neurons, DDIT4 may regulate the timing of Schwann cell myelination by preceding the peak of AKT activation and of DLG1 expression.

In *Ddit4*-null nerves, mTORC1 activation is enhanced, leading to sustained hypermyelination and increased myelin thickness. *Ddit4* loss is not compensated by DLG1, which acts upstream in the pathway and whose expression is stabilized after the rise and fall of *Ddit4* (Cotter et al., 2010). Interestingly, we found that Dlg1 expression is normal in *Ddit4*-null nerves (data not shown). On the other hand, in *Dlg1*-null nerves, mTORC1 activation may induce *Ddit4* upregulation, resulting in a negative feedback loop on mTOR activity and in normal myelin thickness

in adult nerves. Indeed, we found that, along with *Ddit4*, HIF3α is upregulated in *Dlg1*-null nerves at P20 (at both the mRNA and protein level). It is known that mTORC1 activation may lead to HIF1α expression, which in turn induces DDIT4 expression (Ellisen, 2005; Schwarzer et al., 2005). Thus, by analogy, the transient AKT/mTOR activation in *Dlg1*-null nerves may induce both HIF3α and DDIT4 expression downstream of mTORC1, thus eliciting a negative feedback loop on mTOR activity.

The PI3K/AKT pathway and focal hypermyelination
In addition to the regulation of myelin thickness, the PI3K/AKT pathway is believed to control local myelin remodeling and membrane homeostasis (Goebbels et al., 2010, 2012). Loss of either DLG1 (Cotter et al., 2010) or PTEN (Goebbels et al., 2012) and altered PI3K/AKT signaling at regions of noncompact myelin leads to focal hypermyelination, defined as tomacula, recurrent loops, and myelin outfoldings. Accordingly, focal hypermyelination in *Pten*-null mice is ameliorated by rapamycin, a known mTORC1 inhibitor (Goebbels et al., 2012), with a greater effect on tomacula than on myelin outfoldings. This latter observation led to the hypothesis that myelin outfoldings represent a PIP_3-dependent phenomenon, whereas tomacula are linked to the bulk of protein and lipid synthesis that is dependent on mTORC1 activation. This hypothesis is further supported by the fact that loss of either the MTMR2 phospholipid phosphatase (Bolino et al., 2000, 2004) or the guanosine nucleotide exchange factor for cdc42, FGD4 (Stendel et al., 2007; Horn et al., 2012), which binds to phospholipids, provokes demyelinating neuropathies with myelin outfoldings.

Interestingly, in *Ddit4*-null nerves we did not observe signs of focal hypermyelination despite mTORC1 activation and increased myelin thickness. The fact that *Ddit4*-null nerves do not display myelin outfoldings might consistent with the hypothesis that myelin outfolding formation might depend on PIP_3, which is generated upstream of TSC1/2, the target of DDIT4. Further, the fact that we did not observe any tomacula in *Ddit4*-null nerves may suggest that tomacula are dependent on direct AKT activation rather than mTORC1. In this line, in *Pten*-null nerves rapamycin treatment may rescue tomacula because it decreases AKT phosphorylation (473) via the positive feedback between mTORC1, mTORC2, and AKT (Goebbels et al., 2012). Indeed, *Pten*-null mouse nerves treated with rapamycin display decreased levels of AKT phosphorylation at S473 compared with knockout animals treated with vehicle (Goebbels et al., 2012).

References
Abraham RT (2005) TOR signaling: an odyssey from cellular stress to the cell growth machinery. Curr Biol 15:R139–R141. CrossRef Medline
Bolino A, Muglia M, Conforti FL, LeGuern E, Salih MA, Georgiou DM, Christodoulou K, Hausmanowa-Petrusewicz I, Mandich P, Schenone A, Gambardella A, Bono F, Quattrone A, Devoto M, Monaco AP (2000) Charcot-Marie-Tooth type 4B is caused by mutations in the gene encoding myotubularin-related protein-2. Nat Genet 25:17–19. CrossRef Medline
Bolino A, Bolis A, Previtali SC, Dina G, Bussini S, Dati G, Amadio S, Del Carro U, Mruk DD, Feltri ML, Cheng CY, Quattrini A, Wrabetz L (2004) Disruption of Mtmr2 produces CMT4B1-like neuropathy with myelin outfolding and impaired spermatogenesis. J Cell Biol 167:711–721. CrossRef Medline
Bolis A, Coviello S, Bussini S, Dina G, Pardini C, Previtali SC, Malaguti M, Morana P, Del Carro U, Feltri ML, Quattrini A, Wrabetz L, Bolino A (2005) Loss of Mtmr2 phosphatase in Schwann cells but not in motor neurons causes Charcot-Marie-Tooth type 4B1 neuropathy with myelin outfoldings. J Neurosci 25:8567–8577. CrossRef Medline
Bolis A, Coviello S, Visigalli I, Taveggia C, Bachi A, Chishti AH, Hanada T, Quattrini A, Previtali SC, Biffi A, Bolino A (2009) Dlg1, Sec8, and

Mtmr2 regulate membrane homeostasis in Schwann cell myelination. J Neurosci 29:8858–8870. CrossRef Medline

Brafman A, Mett I, Shafir M, Gottlieb H, Damari G, Gozlan-Kelner S, Vishnevskia-Dai V, Skaliter R, Einat P, Faerman A, Feinstein E, Shoshani T (2004) Inhibition of oxygen-induced retinopathy in RTP801-deficient mice. Invest Ophthalmol Vis Sci 45:3796–3805. CrossRef Medline

Cam H, Houghton PJ (2011) Regulation of mammalian target of rapamycin complex 1 (mTORC1) by hypoxia: causes and consequences. Target Oncol 6:95–102. CrossRef Medline

Cotter L, Ozçelik M, Jacob C, Pereira JA, Locher V, Baumann R, Relvas JB, Suter U, Tricaud N (2010) Dlg1-PTEN interaction regulates myelin thickness to prevent damaging peripheral nerve overmyelination. Science 328:1415–1418. CrossRef Medline

DeYoung MP, Horak P, Sofer A, Sgroi D, Ellisen LW (2008) Hypoxia regulates TSC1/2-mTOR signaling and tumor suppression through REDD1-mediated 14-3-3 shuttling. Genes Dev 22:239–251. CrossRef Medline

Ellisen LW (2005) Growth control under stress: mTOR regulation through the REDD1-TSC pathway. Cell Cycle 4:1500–1502. CrossRef Medline

Feltri ML, D'Antonio M, Quattrini A, Numerato R, Arona M, Previtali S, Chiu SY, Messing A, Wrabetz L (1999) A novel P0 glycoprotein transgene activates expression of lacZ in myelin-forming Schwann cells. Eur J Neurosci 11:1577–1586. CrossRef Medline

Goebbels S, Oltrogge JH, Kemper R, Heilmann I, Bormuth I, Wolfer S, Wichert SP, Möbius W, Liu X, Lappe-Siefke C, Rossner MJ, Groszer M, Suter U, Frahm J, Boretius S, Nave KA (2010) Elevated phosphatidylinositol 3,4,5-trisphosphate in glia triggers cell-autonomous membrane wrapping and myelination. J Neurosci 30:8953–8964. CrossRef Medline

Goebbels S, Oltrogge JH, Wolfer S, Wieser GL, Nientiedt T, Pieper A, Ruhwedel T, Groszer M, Sereda MW, Nave KA (2012) Genetic disruption of Pten in a novel mouse model of tomaculous neuropathy. EMBO Mol Med 4:486–499. CrossRef Medline

Guertin DA, Sabatini DM (2007) Defining the role of mTOR in cancer. Cancer Cell 12:9–22. CrossRef Medline

Harrington EP, Zhao C, Fancy SP, Kaing S, Franklin RJ, Rowitch DH (2010) Oligodendrocyte PTEN is required for myelin and axonal integrity, not remyelination. Ann Neurol 68:703–716. CrossRef Medline

Harrington LS, Findlay GM, Lamb RF (2005) Restraining PI3K: mTOR signalling goes back to the membrane. Trends Biochem Sci 30:35–42. CrossRef Medline

Hatanaka M, Shimba S, Sakaue M, Kondo Y, Kagechika H, Kokame K, Miyata T, Hara S (2009) Hypoxia-inducible factor-3alpha functions as an accelerator of 3T3–L1 adipose differentiation. Biol Pharm Bull 32:1166–1172. CrossRef Medline

Horn M, Baumann R, Pereira JA, Sidiropoulos PN, Somandin C, Welzl H, Stendel C, Lühmann T, Wessig C, Toyka KV, Relvas JB, Senderek J, Suter U (2012) Myelin is dependent on the Charcot-Marie-Tooth Type 4H disease culprit protein FRABIN/FGD4 in Schwann cells. Brain 135:3567–3583. CrossRef Medline

Macklin WB (2010) The myelin brake: when enough is enough. Sci Signal 3:pe32. CrossRef Medline

Maiese K, Chong ZZ, Shang YC, Wang S (2013) mTOR: on target for novel therapeutic strategies in the nervous system. Trends Mol Med 19:51–60. CrossRef Medline

Malagelada C, López-Toledano MA, Willett RT, Jin ZH, Shelanski ML, Greene LA (2011) RTP801/REDD1 regulates the timing of cortical neurogenesis and neuron migration. J Neurosci 31:3186–3196. CrossRef Medline

Michailov GV, Sereda MW, Brinkmann BG, Fischer TM, Haug B, Birchmeier C, Role L, Lai C, Schwab MH, Nave KA (2004) Axonal neuregulin-1 regulates myelin sheath thickness. Science 304:700–703. CrossRef Medline

Nave KA (2010) Myelination and support of axonal integrity by glia. Nature 468:244–252. CrossRef Medline

Nave KA, Salzer JL (2006) Axonal regulation of myelination by neuregulin 1. Curr Opin Neurobiol 16:492–500. CrossRef Medline

Pareyson D, Marchesi C (2009) Diagnosis, natural history, and management of Charcot-Marie-Tooth disease. Lancet Neurol 8:654–667. CrossRef Medline

Pereira JA, Lebrun-Julien F, Suter U (2012) Molecular mechanisms regulating myelination in the peripheral nervous system. Trends Neurosci 35:123–134. CrossRef Medline

Pirooznia M, Nagarajan V, Deng Y (2007) GeneVenn—A web application for comparing gene lists using Venn diagrams. Bioinformation 1:420–422. CrossRef Medline

Polak P, Hall MN (2009) mTOR and the control of whole body metabolism. Curr Opin Cell Biol 21:209–218. CrossRef Medline

Roberts SA, Lloyd AC (2012) Aspects of cell growth control illustrated by the Schwann cell. Curr Opin Cell Biol 24:852–857. CrossRef Medline

Sarbassov DD, Ali SM, Sabatini DM (2005) Growing roles for the mTOR pathway. Curr Opin Cell Biol 17:596–603. CrossRef Medline

Schwarzer R, Tondera D, Arnold W, Giese K, Klippel A, Kaufmann J (2005) REDD1 integrates hypoxia-mediated survival signaling downstream of phosphatidylinositol 3-kinase. Oncogene 24:1138–1149. CrossRef Medline

Sheng M, Sala C (2001) PDZ domains and the organization of supramolecular complexes. Annu Rev Neurosci 24:1–29. CrossRef Medline

Sherman DL, Krols M, Wu LM, Grove M, Nave KA, Gangloff YG, Brophy PJ (2012) Arrest of myelination and reduced axon growth when Schwann cells lack mTOR. J Neurosci 32:1817–1825. CrossRef Medline

Shoshani T, Faerman A, Mett I, Zelin E, Tenne T, Gorodin S, Moshel Y, Elbaz S, Budanov A, Chajut A, Kalinski H, Kamer I, Rozen A, Mor O, Keshet E, Leshkowitz D, Einat P, Skaliter R, Feinstein E (2002) Identification of a novel hypoxia-inducible factor 1-responsive gene, RTP801, involved in apoptosis. Mol Cell Biol 22:2283–2293. CrossRef Medline

Sofer A, Lei K, Johannessen CM, Ellisen LW (2005) Regulation of mTOR and cell growth in response to energy stress by REDD1. Mol Cell Biol 25:5834–5845. CrossRef Medline

Stendel C, Roos A, Deconinck T, Pereira J, Castagner F, Niemann A, Kirschner J, Korinthenberg R, Ketelsen UP, Battaloglu E, Parman Y, Nicholson G, Ouvrier R, Seeger J, De Jonghe P, Weis J, Krüttgen A, Rudnik-Schöneborn S, Bergmann C, Suter U, et al. (2007) Peripheral nerve demyelination caused by a mutant Rho GTPase guanine nucleotide exchange factor, frabin/FGD4. Am J Hum Genet 81:158–164. CrossRef Medline

Tanaka T, Wiesener M, Bernhardt W, Eckardt KU, Warnecke C (2009) The human HIF (hypoxia-inducible factor)-3alpha gene is a HIF-1 target gene and may modulate hypoxic gene induction. Biochem J 424:143–151. CrossRef Medline

Taveggia C, Zanazzi G, Petrylak A, Yano H, Rosenbluth J, Einheber S, Xu X, Esper RM, Loeb JA, Shrager P, Chao MV, Falls DL, Role L, Salzer JL (2005) Neuregulin-1 type III determines the ensheathment fate of axons. Neuron 47:681–694. CrossRef Medline

Triolo D, Dina G, Taveggia C, Vaccari I, Porrello E, Rivellini C, Domi T, La Marca R, Cerri F, Bolino A, Quattrini A, Previtali SC (2012) Vimentin regulates peripheral nerve myelination. Development 139:1359–1367. CrossRef Medline

Wrabetz L, Feltri ML, Quattrini A, Imperiale D, Previtali S, D'Antonio M, Martini R, Yin X, Trapp BD, Zhou L, Chiu SY, Messing A (2000) P(0) glycoprotein overexpression causes congenital hypomyelination of peripheral nerves. J Cell Biol 148:1021–1034. CrossRef Medline

Yoshida T, Mett I, Bhunia AK, Bowman J, Perez M, Zhang L, Gandjeva A, Zhen L, Chukwueke U, Mao T, Richter A, Brown E, Ashush H, Notkin N, Gelfand A, Thimmulappa RK, Rangasamy T, Sussan T, Cosgrove G, Mouded M, et al. (2010) Rtp801, a suppressor of mTOR signaling, is an essential mediator of cigarette smoke-induced pulmonary injury and emphysema. Nat Med 16:767–773. CrossRef Medline

Zhou W, Zhang L, Guoxiang X, Mojsilovic-Petrovic J, Takamaya K, Sattler R, Huganir R, Kalb R (2008) GluR1 controls dendrite growth through its binding partner, SAP97. J Neurosci 28:10220–10233. CrossRef Medline

Zolov SN, Bridges D, Zhang Y, Lee WW, Riehle E, Verma R, Lenk GM, Converso-Baran K, Weide T, Albin RL, Saltiel AR, Meisler MH, Russell MW, Weisman LS (2012) In vivo, Pikfyve generates PI(3,5)P2, which serves as both a signaling lipid and the major precursor for PI5P. Proc Natl Acad Sci U S A 109:17472–17477. CrossRef Medline